HHS Public Access

Author manuscript

Nat Neurosci. Author manuscript; available in PMC 2014 June 01.

Published in final edited form as:

Nat Neurosci. 2013 December ; 16(12): 1821–1829. doi:10.1038/nn.3547.

Integration of the olfactory code across dendritic claws of single mushroom body neurons

Eyal Gruntman[1] and **Glenn C. Turner**[*]

Cold Spring Harbor Laboratory, Cold Spring Harbor, New York, USA. and Watson School of Biological Sciences, Cold Spring Harbor Laboratory, Cold Spring Harbor, New York, USA

Abstract

In the olfactory system, sensory inputs are arranged in different glomerular channels, which respond in combinatorial ensembles to the various chemical features of an odor. Here we investigate where and how this combinatorial code is read out deeper in the brain. We exploit the unique morphology of neurons in the mushroom body (MB), which receive input on large dendritic claws. Imaging odor responses of these dendritic claws shows that input channels with distinct odor tuning converge on individual MB neurons. We determined how these inputs interact to drive the cell to spike threshold using intracellular recordings to examine MB responses to optogenetically controlled input. Our results provide an elegant explanation for the characteristic selectivity of MB neurons: these cells receive different types of input, and require those inputs to be coactive in order to spike. These results establish the MB as an important site of integration in the fly olfactory system.

The olfactory system of *Drosophila* is an excellent platform to study how sensory information is transformed as it passes through the successive layers of a neural circuit. Although the fly olfactory circuit is organized similarly to more complex organisms, it is numerically simpler and has been mapped with cellular resolution. Sensory input comes in from a large set of Olfactory Receptor Neurons (ORNs), each of which has a particular chemical sensitivity[1,2]. These inputs are organized into distinct channels in the antennal lobe, as ORNs that express the same type of OR converge to form synapses with a cognate set of Projection Neurons (PNs) in structures termed glomeruli[3]. There are 54 different glomerular channels identified in *Drosophila*[4], and the constellation of different physiochemical features in an odor evokes widely distributed patterns of activity across these channels. In *Drosophila*, the main transformations at the first synapse in the circuit are noise reduction and gain control[5–8]. These transformations distribute activity more uniformly among the glomerular channels in the PN layer than the ORNs[5]. This ensures that the combinatorial capacity of the system is used effectively, and theoretically enables a

[*]Correspondence: turner@cshl.edu.

[1]Present Address: Janelia Farm Research Campus, Howard Hughes Medical Institute, 19700 Helix Drive, Ashburn, VA 20147, USA.

Author Contributions E.G. and G.C.T designed the experiments. E.G. performed the experiments and analyzed the data. E.G. and G.C.T wrote the manuscript.

Competing Financial Interests The authors declare no competing financial interests.

simple linear neural network to more easily discriminate odors[5]. The set of, on average, three PNs present in each glomerular channel[9–11] then transmits information in nearly identical spike trains[12] to downstream brain areas, the lateral horn and mushroom body (MB).

The transformation from the PNs to the MB is of particular interest, because the MB plays an essential role in olfactory learning and memory[13–16]. The MB is composed of 2000 neurons termed Kenyon cells (KCs)[17]. In comparison to PNs, which typically respond to a wide range of odors, KCs have much more odor-selective responses[18–21]. Consequently, the densely combinatorial odor representations in the PN layer are transformed into sparse response patterns across the KC population. The high-specificity of KC responses is thought to underlie the accuracy of memory formation[22], and in fact sparse representations are a general feature of deeper layers of the brain, including the olfactory cortex in mammals[23–25]. However, we understand very little of how KCs achieve such selective responses.

PN-KC synapses are remarkable structures. They are among the largest synapses in the *Drosophila* brain, and have a striking morphology[26,27]. The synaptic terminals of PNs form large ~5 μm boutons which are enwrapped by correspondingly large claw-like dendritic structures of KCs. Although fine distinctions between dendritic specializations can be resolved at high resolution[28], we will refer to these contacts as KC claws, after[ref.26]. Ultrastructural studies have shown that each KC claw contacts a single PN bouton, establishing the claw as the anatomical unit of PN input to these cells[26]. KCs typically have 5 to 7 such claws[26], and a recent study examining the anatomy of PN convergence onto individual KCs indicated that connectivity at this layer was random, and that PNs from different glomerular channels were no more likely to wire together than chance[29].

The unusual morphology of PN-KC connections presented us with the opportunity to investigate the response properties of individual synaptic sites from a functional perspective. First, using *in vivo* dendritic imaging, we directly examined the odor response properties of individual synaptic sites. This approach enabled us to determine whether functionally distinct inputs converge onto individual KCs. Second, to understand how KCs integrate synaptic input, we used optogenetic methods to provide precisely controlled input to the claws, and intracellular recordings to examine the postsynaptic response. The large size of PN-KC synapses enabled us to relate the connectivity we observed anatomically to the functional responses we measured electrophysiologically. We show that KCs receive convergent input from different channels, and require several inputs to be active in order to spike. Notably, we found that these cells achieve their response specificity despite essentially linear additivity of synaptic inputs. Overall, these results demonstrate that a fundamental aspect of the transformation at this layer is the integration of combinatorial patterns of glomerular activity by individual KCs.

RESULTS

Functional imaging of dendritic odor responses

We examined the odor response profiles of individual dendritic claws *in vivo* using two-photon imaging. We used a stochastic genetic approach[30] to label single KCs with both the calcium indicator GCaMP3[31] and the anatomical marker myr-tdTomato. tdTomato enabled easy identification of KC claws *in vivo*, while GCaMP3 reported the postsynaptic response to PN input, which leads to Ca++ influx via calcium-permeable acetylcholine receptors[32] as well as a potential contribution from voltage-gated calcium channels. We examined odor responses of the claws of individually labeled KCs using a panel of 10 different odorants. Figure 1 shows data from an example KC (Fig. 1b). Individual claws exhibited responses that were consistent across multiple presentations (Fig. 1c). Differences between odor response profiles were readily apparent (Fig. 1c and d). For example, claws 1 and 2 showed similar responses to several odors, but could be distinguished by their differential responses to pine and trans-2-hexanal (Fig. 1d Pne and T2h). Even claws in close spatial proximity could exhibit markedly different odor response profiles (claws 3 and 4 in Fig. 1c and d; see also Supplementary Movie 1). Note that for this particular KC, we imaged odor responses of four of its five claws, the claw in the lower left was detected only in a high resolution anatomical z-stack acquired after completing the functional imaging phase of the experiment. Our sampling of KC claws was not comprehensive for every KC, however, our goal was to determine whether or not the claw response profiles we did measure were distinct. Overall, these findings demonstrate that we could reliably measure odor response profiles at individual dendritic sites *in vivo*. Additionally, for this particular KC, we saw that different claws exhibit clearly distinct odor response profiles.

To test whether the convergence of inputs with different odor tuning is a prevailing feature of connectivity in the MB, we examined claw response profiles from a population of KCs (n=34). We commonly observed that claws of the same KC had distinct response profiles (Fig. 2A). In some cases, profiles were completely different (e.g. Fig. 2Ab claws 1 & 4), while in other cases there was a prominent difference in the response to just one odor (e.g. Fig. 2Aa claws 1 & 2, odor 10; same cell as in Fig. 1). We quantified the similarity of claw odor tuning profiles using Pearson's correlation. For each KC, we calculated the correlation between all pairwise combinations of its claws (Fig. 2B). These results indicated that the majority of KCs receive distinct inputs on their claws. We found that 13/34 KC had pairs of claws with correlation below 0, 25/34 KCs had claws with correlation below 0.5, and nearly all KCs (30/34) had claws with correlations below 1. It is important to note that this measure of tuning curve distinctiveness likely represents a lower bound, since we were only able to test 10 odors in these experiments due to photobleaching of the claws. Nevertheless, even within these constraints it was clear that the differences in claw tuning were the dominant feature of the results. These results directly demonstrate that KC dendrites receive convergent inputs with functionally distinct odor tuning properties, corroborating anatomical measures of convergence[29], and showing that KCs meet the first criterion to serve as integrators of the olfactory combinatorial code.

An important question regarding connectivity at this layer is whether there is any relationship between the tuning properties of the different synaptic inputs to a KC. A recent anatomical study indicated that convergence of different PNs is random within the MB[29]. We used our functional characterization to assess the relationship between the odor response properties of different claws on a KC. We found that claws connected to the same KC had more similar odor response profiles than claws from different cells (Fig. 2C). This suggests that PNs with similar tuning profiles have a tendency to connect to the same KC. To account for the possibility that cell-wide changes in membrane potential contribute to a correlation in calcium signals from the claws[33], we constructed tuning profiles using only odors that did not evoke a response at the cell's soma, and then examined the correlation between claw tuning for this reduced set of odors. Of course by doing this we remove not only artifactual correlations that arise in the claws from cell-wide voltage effects, but also true correlations that actually drive somatic responses. Even with this constraint, we observed that tuning curves of claws from the same KC were significantly more correlated than expected by chance. Nevertheless, it remains possible that some feature of cellular physiology other than PN input contributes to the similarity of claw odor tuning. Consequently, we used a more direct approach to test PN-KC connectivity optogenetically, as described in the section below.

We next examined the relationship of claw activation patterns to the somatic calcium signals we measured. Calcium signals at the cell body reflect spiking output in cell types from many different systems[31,34,35], including Projection Neurons in the antennal lobe[36]. Our goal was to determine whether somatic responses required activation of multiple claws, which would indicate that KC responses truly reflect the integration of different input channels. We first determined the number of claws that responded significantly to each odor. Most odors evoked a response in only one or two claws, although there was a wide distribution that ranged up to seven activated claws (Fig. 2D). We then assessed whether the odor also evoked a response from the cell's soma (black boxes in Fig. 2D). This showed that reliable somatic signals typically required activation of multiple claws. Many odors activated one or two claws, but only in a small proportion of those cases was there an accompanying somatic response. In contrast, when an odor activated several claws, somatic responses were observed much more frequently. In fact, odors that activated six or seven claws invariably elicited a somatic response. We note however, that we were unable to establish the relationship between these somatic signals and KC spiking activity. This requires simultaneous imaging and electrophysiological recordings. However, intracellular recordings perturbed the concentration of GCaMP inside the cell, and extracellular recordings were unable to detect KC spikes. Therefore, to directly address the relationship between claw activation and KCs spiking, we combined intracellular recordings with optogenetic stimulation of the inputs.

Optogenetic characterization of PN-KC connectivity

By optogenetically controlling a defined set of PNs, we set about to determine the number and strength of synaptic contacts that are required to evoke a spiking response from a KC (Fig. 3a). We expressed ChR2-YFP in a subset of PNs (3 of 54 glomeruli) using the Mz19-Gal4 driver[37]. Cell-attached recordings in PNs confirmed that light-evoked spiking rates

were similar to those observed during strong odor responses (Fig. 3b), although the dynamics of PN spiking were different, as there was a transient peak in firing that was more prominent with ChR2-based stimulation than in a typical odor response (Fig. 3c)[ref.6]. We performed whole-cell recordings from randomly selected KCs while stimulating the PNs with light pulses of different durations. When we found a connected KC, excitatory post-synaptic responses were clear (Fig. 3d), and in rare cases crossed spike threshold (Fig. 3d and e). By dye-filling the neurons, we were able to determine *post hoc* the number of PN-KC connection sites. We recorded from 80 KCs, of which 39 exhibited a clear synaptic response upon PN stimulation and were adequately filled to visualize the entire dendritic tree.

We then examined the connectivity of these cells with confocal microscopy, identifying PN boutons using the ChR2-YFP label and KC claws via the intracellular dye-fill. PN-KC synapses were clearly visible, as fine KC processes typically formed a grasping or ring-type morphology wrapped around a large globular PN bouton (Fig. 3f). For each KC that exhibited a clear postsynaptic response, we were able to identify at least one site of anatomical contact, and often more. Pharmacological blockade showed that KC responses were mediated by spike-dependent synaptic transmission (Supplementary Fig. 1). We characterized anatomical connectivity in terms of the number of connected claws i.e. a claw contacted by at least one ChR2-expressing PN bouton. We used this definition because, in a small number of cases, a single KC claw exhibited a complex morphology showing contacts with more than one labeled PN bouton (Supplementary Fig. 2). Across our dataset, we found KCs connected via one, two, three and even five claws (n=17 KCs, n=14, n=6 and n=2, respectively; see Supplementary Movie 2).

We compared these results to the connectivity levels expected if PNs converge randomly onto KCs. If connectivity is random, the probability of observing a connection between this set of PNs and a KC is dictated simply by the proportion of all PN boutons that are labeled with the Mz19 driver. We estimated this proportion by directly counting the number of ChR2-expressing boutons in Mz19 flies, and comparing this to the total number of PN boutons from estimates based on PN labeling experiments[18]. This yielded a proportion of 0.05. An independent estimate of the fraction of Mz19 boutons yielded a very similar number of 0.04[ref.38]. We determined the number of connected claws expected for random convergence in a sample of 80 KCs by drawing from a binomial distribution with a probability of connection of 0.05, and the total number of claws for each KC derived from the distribution we observed experimentally (Supplementary Fig. 3). We repeated this process 1000 times and used the results to derive the 99% confidence interval for the number of KCs expected to be found at each connectivity level. This showed that our dataset contained significantly higher numbers of KCs connected via 2, 3, and 5 claws and lower numbers of cells connected via 1 claw than expected from chance (Fig. 3g). Similarly, if we used the connection probability of 0.14 observed in ref.[29], the number of KCs that we found connected via 3 and 5 claws was still higher than expected from random convergence. Overall these results suggest that convergence of this set of PNs is not random, rather that they tend to wire together when they connect to downstream KCs.

Linear additivity of dendritic inputs

Having established anatomical levels of connectivity for each recorded KC, we next examined the postsynaptic response under these stimulation conditions, where PN firing rates are similar to those observed during a strong odor response. KCs responded with an initial depolarization, which subsequently plateaued at a steady membrane potential (Fig. 4a). The plateau occurred roughly 30 ms following stimulus onset, irrespective of the number of activated claws. After this point, even though PN spiking persisted at >100 spikes/sec, the membrane potential got no closer to spike threshold. However, the rate of depolarization within the initial time window was greater when more claws were activated (Supplementary Fig. 4). Consequently, the membrane potential climbed to a higher level for KCs with more activated claws (Fig. 4b). These results suggest that the additivity of inputs from multiple claws is an important determinant of whether cells cross spike threshold. Consequently we turned our attention to how inputs from different claws interact.

To examine the additivity of inputs from different claws, we compared responses of KCs with different numbers of connected claws. Do claws interact synergistically, increasing the drive towards spike threshold when several inputs are activated together, or do they simply add linearly? Synergistic interaction would occur if KCs possess voltage-gated channels that boost response amplitudes, which has been observed in other insects[39–41]. Linear or sublinear additivity would arise if dendrites had purely passive cable properties, as assumed in a previous model of *Drosophila* KCs[18]. We compared the responses observed with multiple active inputs to the response expected from linear summation of a single input (Fig. 4c). Average response amplitudes for KCs connected via one claw were measured for each of the eight photostimulus durations. The response amplitudes expected for KCs connected via 2, 3 or 5 claws were calculated by directly factoring up the amplitudes observed with KCs connected via one claw. These expected values were compared against the experimentally observed results (Fig. 4c). We found that response amplitudes of KCs with two connected claws were not significantly different from doubling the responses observed upon activation of a single claw. For KCs with three connected claws, there was a trend towards a sublinear interaction between claws; this was more prominent with the KCs we found connected via five claws (n=2, an inevitably rare occurrence given that we had to label small numbers of PNs in order to clearly visualize PN-KC synaptic connections). We found no evidence for supralinearity when examining KC responses to any of the different photostimulation regimes. This was true for both prolonged photostimulation durations that lead to a plateaued response, as well as brief stimulations where responses remained in the initial rapid depolarization phase. It is important to note that under these conditions, KCs are receiving high rates of PN input in a short time window. The 25 msec stimulation evokes 7 PN spikes on average during the light pulse, so KCs with multiple PN connections receive high frequency input from several PNs in this brief period. Thus, these conditions were well-suited for observing synergistic interactions that might arise when multiple inputs arrive within a narrow integration window. Nevertheless, we consistently observed that claws interact linearly or sublinearly.

To further address how inputs are integrated in time, we examined KC responses to two precisely timed inputs, current injection at the soma and synaptic stimulation at the

dendrites. We delivered a brief (3 ms) pulse of current together with 10 ms photostimulation, systematically varying the relative timing of these two inputs. This enabled us to test whether there is a particular time window in which these two inputs add synergistically. We compared the experimentally observed responses to that expected from linear summation of responses to isolated synaptic and current stimulation. We found a close match between our observations and the predicted linear response, indicating that KCs are not particularly sensitive to the relative timing of these two inputs (Fig. 4d and e). We also tested whether synaptic responses showed any voltage-dependence. We optogenetically stimulated inputs while holding the KC at different membrane potentials, but found no indication of voltage-dependent amplification of the synaptic response (Supplementary Fig. 5a, b). Additionally, current injection experiments showed no evidence of a non-linear component in the KC membrane potential response, other than spike threshold (Supplementary Fig. 5c, d). Altogether these lines of evidence support a model where synaptic inputs are integrated linearly or sub-linearly, with no apparent voltage-dependent boosting of the synaptic response. Although we found no indication that KCs are especially sensitive to coincident input, interactions across claws are clearly important determinants of response amplitude, and likely contribute to the sparsity of spiking responses in the KCs, which we examined next.

KCs require activation of multiple claws to spike

The most striking feature of this dataset was the scarcity of spiking responses. Although photostimulation evoked large amplitude depolarizations in numerous cases, spiking responses were only rarely observed (Fig. 5a). Only 2 of 39 KCs climbed above spike threshold with sufficient reliability to resemble a significant odor response (i.e. >0.5 spikes/trial). These responses were found only in cells with three or five connected claws (Fig. 5a). We did observe weak light-evoked spiking in two other KCs with lower levels of connectivity; however these cells showed atypical spontaneous firing, and their responses were not as reliable. These results suggested that KCs require strong PN input to multiple claws to evoke a significant spiking response.

To directly address the relationship between numbers of connected claws and spiking, we used the same approach but instead carried out a targeted search for spiking cells. In an entirely separate dataset, we recorded from n=191 randomly selected KCs, searching for cells that spiked reliably in response to photostimulation and then selecting these for anatomical analysis of connectivity. We found 13 reliably responding cells that were adequately dye-filled, example responses are shown in Fig. 5b. We found a range of connectivity amongst these spiking cells, with cells connected to ChR2-expressing PNs via 1, 2, 3, 4 and 6 claws (n=2 KCs, n=3, n=1, n=6 and n=1, respectively). Surprisingly, we found that the number of spikes evoked by photostimulation was not strongly dependent on the number of connected claws (Fig. 5c; linear regression R^2= 0.02). However, although it is rare for a KC to be connected via several claws to the few PNs labeled in this experimental situation, most of the cells that spiked indeed had ChR2-positive connections on multiple claws. We estimated the proportion of KCs we expected to be connected via *n* claws, based on our observations of connectivity from the previous experiment where we characterized connectivity of all synaptically responding KCs. The inset in Fig. 5d shows the proportion of

cells expected for each connectivity level, as well as the proportion of the cells we recorded that exhibited a spiking response. We then used this expected distribution to calculate the proportion of spiking responses for cells with different numbers of connected claws (Fig. 5d main panel). We found a clear relationship between the number of claws receiving strong input and the proportion of KCs exhibiting a spiking response. In particular, there was a prominent increase in the proportion of spiking responses between 3 and 4 contacted claws. KCs have 7 claws on average (Supplementary Fig. 3), so these results suggest that strongly activating more than half of the dendritic inputs is required to drive a KC to spike. The fact that different KCs require different numbers of active inputs may arise in part because there is a wide range of synaptic strengths for individual PN-KC connections (Supplementary Fig. 6).

The outcome of these optogenetic experiments was generally concordant with our results from dendritic imaging (Fig. 2D). In both cases, activation of several claws was required to drive either a spiking response or a somatic calcium signal. However, responses were very rarely observed when a single claw was active, both when imaging odor responses (Fig. 2D) and with optogenetic stimulation (Fig. 5). These results indicate that KCs have a strong but not absolute requirement for activation of multiple claws in order to exhibit a reliable spiking response.

DISCUSSION

There are two basic requirements that must be fulfilled to show that neurons read the combinatorial code of the early olfactory layers: they receive convergent input from functionally distinct glomerular channels, and require activation of multiple inputs in order to respond. Using *in vivo* imaging of the individual synaptic inputs, we found that individual KCs receive inputs with functionally distinct odor response properties. By optogenetically stimulating a defined subset of PNs and intracellularly recording from post-synaptically connected KCs, we have directly shown that several of those inputs must be activated in order to evoke a spiking response in a downstream KC. Our results indicate that KCs respond to specific combinations of coactive glomerular channels. This is likely the basis for their highly stimulus-specific response properties. Notably, we found that synaptic summation is essentially linear in KCs, and multiple lines of evidence indicated KC dendrites have purely passive cable properties. Using patterned photostimulation, others have shown that neurons in olfactory cortex respond selectively to particular patterns of glomerular activation[42]. Thus, the integration of different channels is likely to be a fundamental aspect of the transformation at the third layer of the olfactory system.

Convergence of glomerular channels on KC dendrites

Anatomical studies originally suggested that the MB might be an important site for the convergence of different glomerular channels. PNs send wide-ranging projections within the calyx of the MB, and the synaptic terminals of different PN types intermingle in this area[37,43]. Moreover, single-cell labeling shows that the dendrites of individual KCs extend rather widely within the MB calyx[28,30,44], suggesting they could collect input from different PN types. Retrogradely tracing the inputs to individual KCs indeed showed that PNs of

different glomerular origin converge onto individual KCs[29]. This study found no statistical structure in the probability of different PNs converging onto the same KC, suggesting that connectivity at this layer is random. This result contrasts somewhat with earlier anatomical studies that showed that different PN types show coarsely regionalized projections, although there was extensive overlap between different projection zones.. It has also been shown that different subtypes of KCs tend to innervate particular regions of the MB calyx[37,43]. Consistent with this loose regionalization, one study reported a correlation in the projection patterns of particular types of PNs and KCs[37]. Altogether the evidence from these global mapping studies supported a model where PN-KC connectivity is probabilistic and regionally biased rather than completely random.

We took a functional approach to the question of convergence by directly imaging odor responses of individual synaptic sites. Our results show that functionally distinct inputs converge onto the dendritic trees of individual KCs. When we examined the similarity of odor response profiles for the claws of a given KC, we found that they were more similar to one another than they were to claws from different cells. This suggests that PNs with similar tuning properties have a small but significant tendency to converge onto the same KCs (Fig. 2C). Additionally, when we used ChR2 stimulation to examine the relationship between anatomical and functional connectivity, the levels of connectivity we observed were significantly different from that predicted by random convergence (Fig. 3g). Overall our results were more consistent with the model of regionalized, probabilistic connectivity derived from global mapping of PN and KC projections than entirely random convergence supported by retrograde labeling. Our functional approach may have proved more sensitive to detecting correlations in connectivity than a purely anatomical one; correlated response properties are important determinants of wiring in many neural circuits. Nevertheless, the dominant theme of all these results was that functionally distinct inputs converge onto the dendrites of individual KCs. Convergence is likely a core feature of this layer of the olfactory circuit, as transsynaptic tracing has shown that neurons in the piriform cortex receive mitral cell input originating from several different glomeruli[45].

Linear integration of dendritic inputs

A recent study investigated the input-output transformation of KCs by imaging activity in PN boutons and KC axons[33]. Examining odor-evoked activity in these different cells, this work showed that the summed activity of the PN inputs correlates well with the likelihood of an axonal response in a post-synaptic KC. In contrast, we used an electrophysiological approach to examine synaptic responses to optogenetically controlled PN inputs, enabling us to investigate the integration of inputs from the dendritic claws. By recording from randomly selected KCs and reconstructing their morphology *post hoc*, we established both functional and anatomical measures of connectivity for each cell recorded. Comparing responses of KCs with different levels of connectivity enabled us to determine how different synaptic inputs interact, and to establish the relationship between synaptic input and spiking in these cells.

Dendritic inputs from different sites could interact synergistically, for example by summating to activate voltage-gated channels that boost the synaptic response. Such

synergistic interactions have been observed in mammalian barrel cortex, where coordinated input to different dendritic sites from different sensory modalities elicits a distinct bursting response mode in these cells[46]. Synergistic interactions could make it easier for KCs to respond selectively to particular input patterns; they could enable a clear distinction between activation of a small set of inputs that is not sufficient to bring the cell to spike and activation of a larger, supra-threshold number of inputs. Electrical stimulation experiments in locust KCs showed that synaptic responses are amplified and temporally sharpened by a voltage-dependent mechanism[39,40]. In contrast, our results with Drosophila KCs showed that claws interact linearly when small numbers are coactive, and sub-linearly when larger numbers are stimulated, likely due to shunting effects on the dendritic tree. Note that our stimulation conditions were designed to deliver high frequency PN input in a narrow time window, conditions that are well-suited to reveal synergistic interactions between coincident input. In separate experiments, we examined the interaction between two precisely timed inputs, synaptic stimulation at the dendrites and current injection at the soma (Fig. 4d & e). We examined the additivity of these inputs at a variety of different relative timings, and again found no evidence for synergistic effects that would indicate heightened sensitivity to coincident input. Rather our results are consistent with a model where KC dendrites serve as passive cables that convey and integrate synaptic input. Interestingly, this may enable KCs to take advantage of the format of PN population activity. The antennal lobe transforms olfactory signals so that population representations are more linearly separable in the PNs than in the ORNs[6]. By acting as linear integrators, the KC dendrites would be well-suited to separate distinct PN activity patterns.

Our results here are reminiscent of findings from third order neurons in vertebrates. A recent study of cells in the dorsal telencephalon (Dp) of zebrafish showed that these cells exhibit no special sensitivity to synchronous mitral cell inputs[47]. Rather, input synchronization was important to control the precise timing of Dp spikes. Similarly, in mammalian olfactory cortex, synaptic inputs arrive in alternating waves of excitation and inhibition, which enforce temporally precise spiking, phase-locked to this oscillation cycle[25]. In the case of the Dp neurons, the main factor driving cells to spike threshold was a large, slow depolarization, while the oscillatory synaptic drive governed the timing of spikes. This is very similar to intracellular recordings of KC odor responses: large depolarizations are observed, with high frequency (although non-periodic) fluctuations riding on top[18,48]. As such, it seems likely that the main factor driving KCs to spike threshold in *Drosophila*, like Dp neurons, is the slow wave of depolarization that arises from the summation of PN input from several dendritic claws.

Kenyon cells detect coactive input from multiple channels

The linear/sublinear additivity of claws is likely an important factor contributing to the sparsity of KC spikes. When examining synaptic responses, we found only a few cases where PN stimulation evoked a response that was consistently above spike threshold in the postsynaptic KC. These KCs were connected via several claws, three claws for one cell, five for the other. To characterize the relationship between connectivity and spiking, we carried out an extensive series of recordings in which we searched specifically for KCs that spike in response to photostimulation. We found a range of connectivity within the set of responding

cells. We compared across these different cells to examine the effects of increasing connectivity on spiking characteristics of KCs. Surprisingly, we found no correlation between number of contacted claws and the magnitude of the spiking response. KCs tended to either respond or not, similar to the odor-evoked responses of these cells, which also do not span a wide range of spike rates[18]. However, when we examined the likelihood of KC responses as a function of number connected claws, we saw a strong relationship. This analysis showed there was a marked increase in the proportion of responding cells receiving input on 4 or more claws. KCs typically have 5–7 claws, so this suggests that the majority of a KCs claws need to be coactive in order to evoke a odor-like response.

This requirement was not absolute however, as we found cells with reliable spiking responses with lower levels of connectivity, and even a very small number of KCs that spiked when connected via only a single claw (2 of 191 total recorded KCs). While it is possible that some KCs require activation of all their claws, it seems likely that most KCs require only a subset of their inputs to be active in order to spike. As there are many different PN input patterns that could activate a subset of the KCs claws, these results indicate that KCs encode input patterns in a degenerate manner, and that several different input patterns could effectively drive the cell. This is consistent with the odor response properties of KCs; although these cells are much more odor-selective than PNs, they do occasionally respond to multiple odors[18,19,48]. Thus, although KCs' requirement for multiple coactive inputs certainly contributes to their stimulus-selectivity, that selectivity is not absolute. Moreover, inhibitory circuit elements could potentially play an important role in controlling this selectivity, a possibility we have not addressed here[49]. Together, these considerations indicate that KCs are likely to be degenerate decoders that respond to several related PN response patterns.

Our study shows that KCs derive their highly specific response properties by integrating over diverse input channels, effectively reading the combinatorial odor code. Why would such selective responses be constructed from synaptic inputs with widely divergent tuning? One possibility is that it gives the MB the flexibility to support olfactory learning. Since each KC is connected to inputs with very different odor tuning, adjusting the synaptic strength of one of the inputs could dramatically alter the cell's response properties. Additionally, this convergent connectivity is likely important to diversify the odor response properties of the KCs relative to the PNs. This diversification could enable the network to transition from broadly tuned PNs to narrowly tuned KCs[18–20,50] while maintaining the capacity to represent many different odors.

METHODS

In vivo Dendritic Imaging

Generating GCaMP3 expression in individual KCs—To label small numbers of KCs with GCaMP3 and myr-tdTomato, we used a recombination-based approach known as Mosaic Analysis with a Repressible Cell Marker (MARCM)[30]. We constructed heterozygous flies by crossing a reporter strain of genotype: *hs-FLP, tubP-Gal80, neoFRT(19A); UAS-GCaMP3; myr-tdTomato/TM3, ser* to a driver strain of genotype: *neoFRT; OK107-Gal4.* (*UAS-myr-tdTomato* was provided courtesy of Tom Clandinin,

Stanford.) Mitotic recombination between the FRT sites in these animals causes loss of the Gal80 repressor, releasing expression of GCaMP3 and myr-tdTomato by the OK107-Gal4 driver. Recombination is initiated by flippase, which is under control of a heat-shock inducible promoter. Although the recombination and subsequent expression occurs stochastically in a subset of KCs, the size of the set of labeled KCs is influenced by the duration of the heat-shock induction. To generate sparsely labeled animals with an experimentally practicable frequency, we empirically derived the following labeling procedure.

We collected eggs laid in a 2 hour time window, transferred them to a vial of fresh food and left them to develop for 4 days at 25°C. Heat shock was carried out by transferring larvae in food vials to a 37°C water bath for 20–30 min. The brief duration of this heat shock increased the probability of labeling only one or two KCs per MB. We conducted the heat shock 4 days post-hatching in order to increase the probability of labeling α′/β′ Kenyon cells, which are born at this time during development[51] and are known to be more responsive to odors than other KC types[18]. This protocol enabled us to label one or two KCs in, on average, one of every four flies (i.e. eight brain hemispheres). We imaged dendritic responses in 2–5 day old female flies produced by this protocol.

Animal preparation—Two to five day old female flies were prepared for imaging as described[19]. To minimize brain movement within the head capsule, it was sometimes necessary to immobilize the proboscis by epoxying it within its socket. The peri-neural sheath was left intact for all imaging experiments. Extracellular saline contained (in mM) 103 NaCl, 3 KCl, 4 MgCl2, 1.5 CaCl2, 26 NaHCO3, 5 N-tris(hydroxymethyl) methyl-2-aminoethane-sulfonic acid, 1 NaH2 PO4,10 trehalose, and 10 glucose. Saline osmolarity was adjusted to 275 mOsm with sucrose if necessary and equilibrated to pH 7.3 by constantly bubbling with a mixture of 95% O2-5% CO2.

Odor delivery—Odor stimuli were: 1-hexanol (Sigma), 2-phenylethanol, pentyl acetate, methyl benzoate, trans-2-hexanal, geraniol, apple cider vinegar (Richfood) and three essential oils (Aura Cacia): peppermint, pine and orange. Odors were presented in pseudo-random order within blocks; no odor was presented twice in succession. At least three blocks of trials were presented in every experiment. Odors were delivered at a concentration of 5% saturated vapor using a custom-built odor delivery system[19]. We chose this relatively high odor concentration to increase the likelihood of evoking odor responses in the KCs. Overall air flow was 1 L/min. Odor pulses were 1 sec in duration, and the inter-stimulus interval was 18 sec. Odor delivery was monitored using a photoionization detector (PID; Aurora Scientific), and was highly reliable across trials.

Dendritic calcium imaging—Two-photon imaging was carried out using a Prairie Ultima system (Prairie Technologies) and a Chameleon Ti-Sapphire laser (Chameleon XR, Coherent Inc.) tuned to 920 nm. Laser power was adjusted to deliver the minimal amount of power that still allowed detection of the dendritic processes based on myr-tdTomato fluorescence (no more than 8 mW at the sample). Emission fluorescence was collected through a HQ607/45-2p filter (Chroma Technologies). All images were acquired using the Olympus LUMPlanFl/IR 60×, 0.90 NA water immersion objective. Imaging planes were

selected to maximize the cross-sectional area of each claw. Typical frames were 120 X 150 pixels, acquired with a pixel dwell time of 4 μs, yielding frame rates near 12 Hz. Frame scans were acquired as 11 sec trials, from 4 sec prior to odor valve opening, though the 1 sec odor pulse, until 6 sec after odor valve closing.

Imaging analysis—Data were analyzed using custom routines written in Matlab (The Mathworks). To correct for motion artefacts, we aligned frames from the same trial by calculating a translational-based discrete Fourier analysis[52] on the anatomical signal from the red channel and applying the translation to both red and green channels. Since each individual frame was too noisy to allow for movement correction, three sequential frames were averaged, then median filtered, and the resulting translation was applied to the middle frame.

A Region of Interest (ROI) was selected manually around each claw using the red myr-tdTomato signal. The boundaries of the ROI were tailored to the image of the claw by examining pixel intensity values throughout the duration of the experiment. Pixels that never exhibited intensity value greater than those observed in a 'background' area of the frame were excluded from the claw ROI.

We quantified claw activity in the following steps: first the mean fluorescence signal (F) from all pixels within the ROI was calculated for the green (GCaMP) and red (myr-tdTomato) channels individually. Second, fluorescence values were adjusted for photo-bleaching by fitting an exponential function to the fluorescence values recorded on each trial. The correction was only applied to the red channel, since the green channel did not display photo-bleaching (additionally, the green channel values were subtracted from green baseline, therefore it is of less consequence). Third, to exclude movement artefacts, frames in which the red signal was 2 standard deviations below the average were discarded from the time series. If a trial had more than 65% of frames discarded from the baseline or response periods, the entire trial was discarded. Fourth, a $\Delta F_{Green}/F_{red}$ value was calculated for each frame using the formula: $(F(t)_{Green} - Fb_{Green})/F(t)_{Red}$., where F(t) is the fluorescence signal for a frame at time (t) and Fb is the baseline fluorescence (averaged over the 3 sec prior to odor valve opening). We quantified the overall magnitude of odor responses for each ROI by summing ΔG/R values that were greater than two standard deviations above baseline. If no such frames were found, the response was defined as zero; we made no attempt to calculate negative responses.

Calculating tuning correlations with random connectivity—To generate the distribution of claw tuning curve correlations assuming random connectivity shown in Fig. 2C, we first pooled together all the claw tuning curves. We then simulated a population of 34 cells by drawing response tuning curves from the pool based on the experimentally determined distribution of KC claws (Supplementary Fig. 3). All pairwise correlations within the this set of simulated KCs was calculated, and this process was repeated 1000 times to determine the variance of the expected results.

ChR2-based PN Stimulation

Fly Strains—For PN photostimulation experiments, we used 4 to 7 day old heterozygous females generated by crossing *Mz19-Gal4*[ref. 37,53] to *UAS-ChR2-YFP* (line C in ref.[54]). This driver labels 13 PNs from 3 different glomeruli (DA1, DC3 and VA1d). Progeny were collected on the day of eclosion and transferred onto agar plates where they were supplied with yeast paste supplemented with 5 mM all-trans-retinal (Sigma). Flies fed on these plates for 3 days at 25°C in the dark to maintain the retinal in the all-trans state. The plates were supplemented with fresh retinal-containing yeast paste every 2–3 days, and flies were used for recordings during the next 2–3 days.

Animal Preparation—Flies were prepared as for imaging experiments, except the antennae were surgically removed to reduce baseline synaptic activity[55] and facilitate the detection of light-evoked responses. Additionally, the peri-neural sheath was carefully removed with fine forceps. For cell-attached recordings of PNs, the head was tilted backwards and the antennae positioned on the upper side of the recording platform. The cuticle between the eyes and the antennae was then removed completely to expose the antennal lobes. Extracellular saline was identical to the saline used in the dendritic imaging experiment, except for the experiments in Supplementary Fig. 1, when it was supplemented with either 1μM TTX or 100μM Mecamylamine. The saline in the recording electrode contained (in mM) 125 L-K aspartate, 10 HEPES, 1.1 EGTA, 0.1 CaCl2, 4 MgATP, 0.5 Na3GTP, and 250μM Alexa Fluor 568 hydrazide (Invitrogen) that was added fresh to the solution for a final adjusted osmolarity of 265 mOsm.

Light stimulation—Light stimulation was delivered using a blue LED (470 nm) mounted on a collimated holder (Thorlabs LEDC1) in the fluorescence light path of an Olympus BX51 microscope. We controlled the light using a driver (Thorlabs LEDD1B) to provide 1 Amp current to the LED and custom written Matlab routines to control stimulus timing. Light stimulation was delivered through a LUMPlanFl/IR 60×, 0.90 NA water immersion objective, providing extensive wide-field illumination of the preparation. Photostimulus durations of 1, 2, 5, 10, 25, 50, 100 and 250 ms were presented in a randomly interleaved fashion.

Electrophysiology—Whole cell recordings from KCs were as described[18] except the saline in the recording pipette contained 250 μM Alexa 568 hydrazide (Molecular Probes), which was added fresh to the internal solution from a 1 mM stock immediately before each experiment (internal solution adjusted so final osmolarity was 265 mOsm).

We assessed the quality of KC recordings by injecting each cell with a current ramp at three separate times during the experiment and determined spiking threshold. Cells in which spikes could not be detected were excluded from the analysis. Although some cells that showed no response to photostimulation were analyzed fully in the dataset, we often aborted the recordings of cells that did not show any sign of functional connection during the recording session. If, after three repeats of the entire photostimulation protocol, there was no obvious response in the KC, the recording was typically aborted. For the photostimulation experiment targeting spiking cells (Fig. 5c and d), 10 repeats of 25ms, and 250ms were

given at the beginning of the recording and if no spikes were observed the recording was aborted. 2 KCs that did not spike were included in the dataset as negative controls (so as not to bias the connection count), one did not provide a good enough fill, and the other had 1 connection.

Cell-attached PN recordings were done under similar conditions only with the fly's head tilted backwards and marginally wider pipettes to minimize spontaneous break-in. Typical seal resistances were 60–100 MOhm. A strong current pulse (500 pA for 500 msec) was delivered at the end of each recording to verify that spikes could not be evoked and therefore no spontaneous break-in had occurred.

Analysis—We calculated the magnitude of KC responses to photostimulation by averaging membrane potential traces for each stimulus duration and then measuring the difference between the peak of the response and baseline. Spiking responses were quantified by determining the number of spikes in a time window from stimulus onset to 200 ms after stimulus offset and then subtracting mean baseline spiking, calculated in an identical time interval prior to stimulus onset (although most cells had a baseline rate of zero).

To quantify the range of PN-KC synaptic strengths, we measured the amplitudes of individual EPSPs from KCs connected via a single claw. Using the 25 ms photostimulation trials, we selected individual trials in which EPSPs were identifiable, manually marked the base and peak of the first EPSP in each train, and took the difference as the EPSP amplitude.

Imaging PN-KC Connections—To effectively visualize anatomical connectivity between PNs and KCs, we dye-filled KCs intracellularly with Alexa Fluor 568 hydrazide (Invitrogen), which was necessary to discern their fine dendritic processes. However, combining these intracellular fills with standard immunocytochemistry protocols caused a dramatic reduction in the signal from the dye. Consequently, we directly imaged brains following a brief fixation. Immediately after the recording, the brain was dissected out of the head capsule and transferred to 0.1 M phosphate buffer pH 7.3. Paraformaldehyde (Electron Microscopy Sciences) was then added to a final concentration of 4% and the brain was rocked for 10 min at room temperature. After this fixation, the brain was washed three times with phosphate buffer, mounted directly on a slide with Vectashield (Vector Laboratories) and imaged. Confocal stacks (0.4 μm z-steps) were acquired with a Zeiss LSM-510 using a 63× 1.4 NA oil immersion objective. Connections between PN boutons and KC claws were scored blind to the results of functional connectivity, using ImageJ software[56].

Analyzing Connectivity—To estimate the connectivity levels expected from random convergence of PNs (Fig. 3g), we calculated connection probability using two independent measures of the proportion of PN boutons labeled with the Mz19 driver. First, we manually counted the number of ChR2-expressing PN boutons in *Mz19-Gal4; UAS-ChR2-YFP* flies. This was done using the imageJ Cell Counter plugin (http://rsbweb.nih.gov/ij/plugins/cell-counter.html). The total number of PN boutons in the MB was taken from published counts[18]. Calculated this way, we estimated the proportion of Mz19 boutons at 0.05. A previously published estimate of the proportion of Mz19 boutons across several brains

yielded a median of 0.04[ref. 38]. For our calculations, we have used a probability of connection of 0.05 (upper quartile in ref. [38]).

We used this connection probability to estimate the number of KC claws connected to Mz19 PNs. We simulated a population of 80 KCs, drawing the total numbers of claws on each cell from the probability distribution we measured experimentally (Supplementary Fig. 3). We then calculated the number of contacted claws for each of these cells using the binomial distribution with p=0.05 and n the number of claws on each of the cells. This simulated the number of connected claws expected in a single experiment with 80 KCs. We repeated this simulated experiment 1000 times to determine the variance of the expected results. In this way, we estimated the distribution of the number of connected claws expected if connectivity is random.

To generate the distribution of connectivity levels expected for the photostimulation experiment where we searched for spiking cells (Fig. 5d), we derived a parametric description of the connectivity levels we observed in our first photostimulation dataset. We fit the observed distribution of connected claw numbers using the EzyFit package from Frederic Moisy on the Matlab file exchange (http://www.mathworks.com/matlabcentral/fileexchange/10176-ezyfit-2-41). We tested all the discrete distributions and found the geometric distribution was the closest fit. These parameters were then used to simulate a population of 80 KCs with numbers of connected claws drawn from a geometric distribution. We generated 1000 such samples of 80 KCs to establish the mean and variance of the number of those 80 cells connected with different numbers of claws. Note that we used the binomial distribution for Figure 3g since our objective was to test the observed distribution against the distribution expected from random connectivity, while in Figure 5d we used the geometric distribution, since our objective was to fit the data as accurately as possible.

Supplementary Material

Refer to Web version on PubMed Central for supplementary material.

Acknowledgments

We thank Dan Tracey, Tom Clandinin and the Bloomington *Drosophila* Stock Center for fly strains, Greg Jefferis for advice on MARCM experiments, Toshihide Hige for support with whole-cell recordings, and Tom Clandinin, Vivek Jayaraman, Greg Jefferis, Sachin Ranade, Yi Zhong and members of the Turner lab for comments on the manuscript.

E.G. is supported by the Elisabeth Sloan Livingston fellowship from the Watson School of Biological Sciences. This work was funded by NIH grant R01 DC010403-01A1.

References

1. Hallem EA, Carlson JR. Coding of odors by a receptor repertoire. Cell. 2006; 125:143–160. [PubMed: 16615896]
2. Benton R, Vannice KS, Gomez-Diaz C, Vosshall LB. Variant ionotropic glutamate receptors as chemosensory receptors in Drosophila. Cell. 2009; 136:149–162. [PubMed: 19135896]
3. Vosshall LB, Wong AM, Axel R. An olfactory sensory map in the fly brain. Cell. 2000; 102:147–159. [PubMed: 10943836]

4. Chou YH, et al. Diversity and wiring variability of olfactory local interneurons in the Drosophila antennal lobe. Nat Neurosci. 2010; 13:439–449. [PubMed: 20139975]
5. Olsen SR, Bhandawat V, Wilson RI. Divisive normalization in olfactory population codes. Neuron. 2010; 66:287–299. [PubMed: 20435004]
6. Bhandawat V, Olsen SR, Gouwens NW, Schlief ML, Wilson RI. Sensory processing in the Drosophila antennal lobe increases reliability and separability of ensemble odor representations. Nat Neurosci. 2007; 10:1474–1482. [PubMed: 17922008]
7. Olsen SR, Wilson RI. Lateral presynaptic inhibition mediates gain control in an olfactory circuit. Nature. 2008; 452:956–960. [PubMed: 18344978]
8. Root CM, et al. A presynaptic gain control mechanism fine-tunes olfactory behavior. Neuron. 2008; 59:311–321. [PubMed: 18667158]
9. Wong AM, Wang JW, Axel R. Spatial representation of the glomerular map in the Drosophila protocerebrum. Cell. 2002; 109:229–241. [PubMed: 12007409]
10. Marin EC, Jefferis GSXE, Komiyama T, Zhu H, Luo L. Representation of the glomerular olfactory map in the Drosophila brain. Cell. 2002; 109:243–255. [PubMed: 12007410]
11. Yu H-H, et al. A complete developmental sequence of a Drosophila neuronal lineage as revealed by twin-spot MARCM. PLoS Biol. 2010; 8
12. Kazama H, Wilson R. Origins of correlated activity in an olfactory circuit. Nat Neurosci. 2009; 12:1136–1144. [PubMed: 19684589]
13. Keene AC, Waddell S. Drosophila olfactory memory: single genes to complex neural circuits. Nat Rev Neurosci. 2007; 8:341–354. [PubMed: 17453015]
14. Davis RL. Traces of Drosophila memory. Neuron. 2011; 70:8–19. [PubMed: 21482352]
15. Heisenberg M. Mushroom body memoir: from maps to models. Nat Rev Neurosci. 2003; 4:266–275. [PubMed: 12671643]
16. Fiala A. Olfaction and olfactory learning in Drosophila: recent progress. Curr Opin Neurobiol. 2007; 17:720–726. [PubMed: 18242976]
17. Aso Y, et al. The mushroom body of adult Drosophila characterized by GAL4 drivers. J Neurogenet. 2009; 23:156–172. [PubMed: 19140035]
18. Turner GC, Bazhenov M, Laurent G. Olfactory representations by Drosophila mushroom body neurons. J Neurophysiol. 2008; 99:734–746. [PubMed: 18094099]
19. Honegger KS, Campbell RAA, Turner GC. Cellular-resolution population imaging reveals robust sparse coding in the Drosophila mushroom body. J Neurosci. 2011; 31:11772–11785. [PubMed: 21849538]
20. Perez-Orive J, et al. Oscillations and sparsening of odor representations in the mushroom body. Science. 2002; 297:359–365. [PubMed: 12130775]
21. Szyszka P, Ditzen M, Galkin A, Galizia CG, Menzel R. Sparsening and temporal sharpening of olfactory representations in the honeybee mushroom bodies. J Neurophysiol. 2005; 94:3303–3313. [PubMed: 16014792]
22. Laurent G. Olfactory network dynamics and the coding of multidimensional signals. Nat Rev Neurosci. 2002; 3:884–895. [PubMed: 12415296]
23. Stettler DD, Axel R. Representations of odor in the piriform cortex. Neuron. 2009; 63:854–864. [PubMed: 19778513]
24. Miura K, Mainen ZF, Uchida N. Odor representations in olfactory cortex: distributed rate coding and decorrelated population activity. Neuron. 2012; 74:1087–1098. [PubMed: 22726838]
25. Poo C, Isaacson JS. Odor representations in olfactory cortex: ‘sparse’ coding, global inhibition, and oscillations. Neuron. 2009; 62:850–861. [PubMed: 19555653]
26. Leiss F, Groh C, Butcher NJ, Meinertzhagen IA, Tavosanis G. Synaptic organization in the adult Drosophila mushroom body calyx. J Comp Neurol. 2009; 517:808–824. [PubMed: 19844895]
27. Butcher NJ, Friedrich AB, Lu Z, Tanimoto H, Meinertzhagen IA. Different classes of input and output neurons reveal new features in microglomeruli of the adult Drosophila mushroom body calyx. J Comp Neurol. 2012; 520:2185–2201. [PubMed: 22237598]

28. Strausfeld NJ, Sinakevitch I, Vilinsky I. The mushroom bodies of Drosophila melanogaster: an immunocytological and golgi study of Kenyon cell organization in the calyces and lobes. Microsc Res Tech. 2003; 62:151–169. [PubMed: 12966500]
29. Caron SJC, Ruta V, Abbott LF, Axel R. Random convergence of olfactory inputs in the Drosophila mushroom body. Nature. 2013; 497:113–117. [PubMed: 23615618]
30. Lee T, Luo L. Mosaic analysis with a repressible cell marker for studies of gene function in neuronal morphogenesis. Neuron. 1999; 22:451–461. [PubMed: 10197526]
31. Tian L, et al. Imaging neural activity in worms, flies and mice with improved GCaMP calcium indicators. Nat Methods. 2009; 6:875–881. [PubMed: 19898485]
32. Oertner TG, Brotz TM, Borst A. Mechanisms of dendritic calcium signaling in fly neurons. J Neurophysiol. 2001; 85:439–447. [PubMed: 11152745]
33. Li H, Li Y, Lei Z, Wang K, Guo A. Transformation of odor selectivity from projection neurons to single mushroom body neurons mapped with dual-color calcium imaging. Proc Natl Acad Sci USA. 2013; 110:12084–12089. [PubMed: 23818618]
34. Yaksi E, Friedrich RW. Reconstruction of firing rate changes across neuronal populations by temporally deconvolved Ca2+ imaging. Nat Methods. 2006; 3:377–383. [PubMed: 16628208]
35. Akerboom J, et al. Optimization of a GCaMP Calcium Indicator for Neural Activity Imaging. J Neurosci. 2012; 32:13819–13840. [PubMed: 23035093]
36. Jayaraman V, Laurent G. Evaluating a genetically encoded optical sensor of neural activity using electrophysiology in intact adult fruit flies. Frontiers in Neural Circuits. 2007; 1:3. [PubMed: 18946545]
37. Tanaka NK, Awasaki T, Shimada T, Ito K. Integration of chemosensory pathways in the Drosophila second-order olfactory centers. Curr Biol. 2004; 14:449–457. [PubMed: 15043809]
38. Kremer MC, et al. Structural Long-Term Changes at Mushroom Body Input Synapses. Curr Biol. 2010; 20:1938–1944. [PubMed: 20951043]
39. Laurent G, Naraghi M. Odorant-induced oscillations in the mushroom bodies of the locust. Journal of Neuroscience. 1994; 14:2993–3004. [PubMed: 8182454]
40. Perez-Orive J, Bazhenov M, Laurent G. Intrinsic and circuit properties favor coincidence detection for decoding oscillatory input. J Neurosci. 2004; 24:6037–6047. [PubMed: 15229251]
41. Demmer H, Kloppenburg P. Intrinsic membrane properties and inhibitory synaptic input of kenyon cells as mechanisms for sparse coding? J Neurophysiol. 2009; 102:1538–1550. [PubMed: 19553491]
42. Davison IG, Ehlers MD. Neural circuit mechanisms for pattern detection and feature combination in olfactory cortex. Neuron. 2011; 70:82–94. [PubMed: 21482358]
43. Lin HH, Lai JSY, Chin AL, Chen YC, Chiang AS. A map of olfactory representation in the Drosophila mushroom body. Cell. 2007; 128:1205–1217. [PubMed: 17382887]
44. Zhu S, Chiang AS, Lee T. Development of the Drosophila mushroom bodies: elaboration, remodeling and spatial organization of dendrites in the calyx. Development. 2003; 130:2603–2610. [PubMed: 12736205]
45. Miyamichi K, et al. Cortical representations of olfactory input by trans-synaptic tracing. Nature. 2011; 472:191–196. [PubMed: 21179085]
46. Xu NL, et al. Nonlinear dendritic integration of sensory and motor input during an active sensing task. Nature. 2012; 492:247–251. [PubMed: 23143335]
47. Blumhagen F, et al. Neuronal filtering of multiplexed odour representations. Nature. 2011; 479:493–498. [PubMed: 22080956]
48. Murthy M, Fiete I, Laurent G. Testing Odor Response Stereotypy in the Drosophila Mushroom Body. Neuron. 2008; 59:1009–1023. [PubMed: 18817738]
49. Papadopoulou M, Cassenaer S, Nowotny T, Laurent G. Normalization for sparse encoding of odors by a wide-field interneuron. Science. 2011; 332:721–725. [PubMed: 21551062]
50. Wilson RI, Turner GC, Laurent G. Transformation of olfactory representations in the Drosophila antennal lobe. Science. 2004; 303:366–370. [PubMed: 14684826]

51. Lee T, Lee A, Luo L. Development of the Drosophila mushroom bodies: sequential generation of three distinct types of neurons from a neuroblast. Development. 1999; 126:4065–4076. [PubMed: 10457015]

52. Guizar-Sicairos M, Thurman ST, Fienup JR. Efficient subpixel image registration algorithms. Opt Lett. 2008; 33:156–158. [PubMed: 18197224]

53. Ito K, Urban J, Technau GM. Distribution, classification, and development of Drosophila glial cells in the late embryonic and early larval ventral nerve cord. Roux's Arch Dev Biol. 1995; 204:284–307.

54. Hwang RY, et al. Nociceptive neurons protect Drosophila larvae from parasitoid wasps. Curr Biol. 2007; 17:2105–2116. [PubMed: 18060782]

55. Olsen SR, Bhandawat V, Wilson RI. Excitatory interactions between olfactory processing channels in the Drosophila antennal lobe. Neuron. 2007; 54:89–103. [PubMed: 17408580]

56. Abramoff MD, Magalhães PJ, Ram SJ. Image processing with ImageJ. Biophotonics International. 2004; 11:36–42.

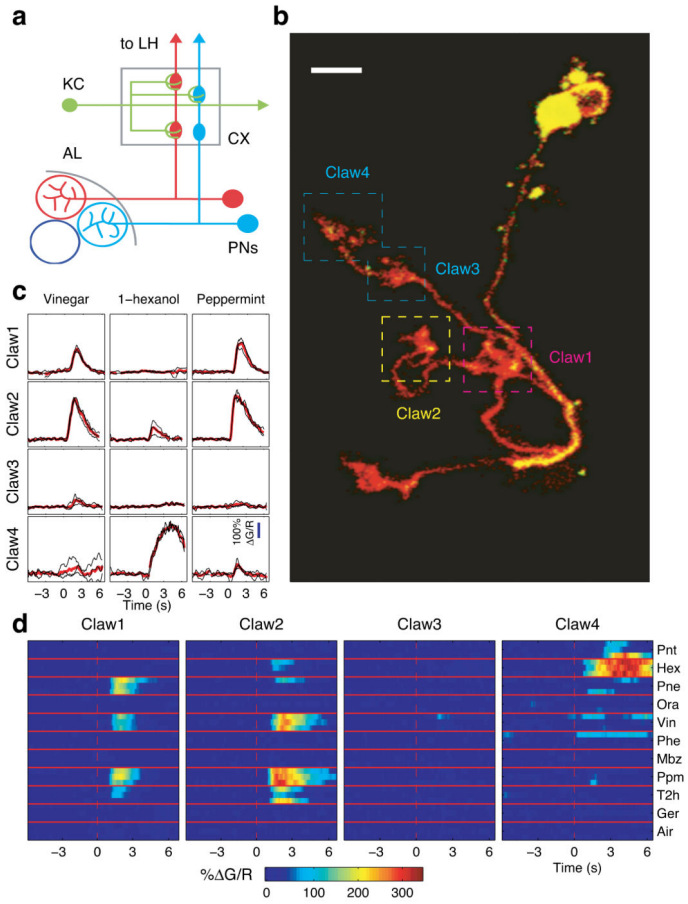

Figure 1. Imaging dendritic claws of Kenyon cells reveals distinct odor responses

a) Schematic of the *Drosophila* olfactory circuit. Projection Neurons (PNs) in the antennal lobe (AL) send axons to mushroom body calyx (CX) where they make synaptic contact with Kenyon cells (KCs) via large synaptic boutons that are enwrapped by claw-shaped dendrites. *b)* An example KC with five claws labeled with GCaMP3 and the anatomical marker myr-tdTomato. Image is a projection of a z-series that bracketed the cell body and dendritic region of the MB. Boxes demarcate claws whose odor responses were characterized. Note that, in this particular example, we imaged four of the total five claws (fifth claw located on bottom left, not demarcated). Scale bar, 5 μm.

c) Odor response timecourses (ΔG/R) from dendritic claws numbered in **b**. Responses from individual trials are shown in black (n=3), mean responses in red. Odor valve opening is at t=0. Note distinct odor responses in claws 3 and 4 despite their close physical proximity.

d)Δ G/R responses of each claw from **b** to panel of 10 odorants (3 trials per odor).

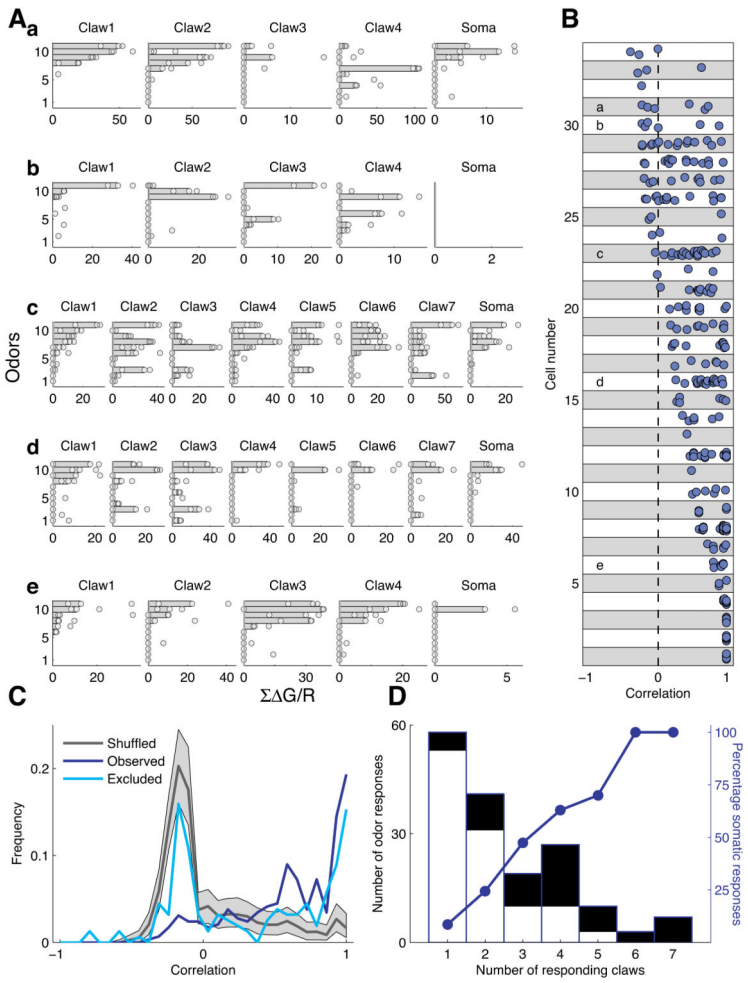

Figure 2. KC dendrites collect inputs with diverse odor response profiles

A) Odor response profiles of dendritic claws and the cell bodies from five different KCs (**a–e**). All the claws imaged from a single KC are presented in a single row with each sub-panel depicting the results from a single claw (or soma). Points are responses to a single odor presentation, while bars represent the median. Claws are arranged by the order in which they were imaged; odors are ordered for each cell based on the sorted response of the first imaged claw.

B) Pairwise correlations of claw response profiles (n=34 KCs). Correlation of claws from the same KC are demarcated within a box. KCs are ordered according to the minimal correlation score. Of the 34 total KCs, 13 cells had pairs of claws with correlation below 0, while 25 cells had pairs with correlation below 0.5. Letters refer to the KCs shown in **A**.

C) Correlation between claws is higher than expected by chance. Shuffled dataset was generated by calculating correlations on random sets of claws (see Methods). Excluded dataset was generated by excluding odors that evoked somatic responses for each KC separately and calculating pairwise correlation on the reduced response profiles. Note that the negative correlation peak is a result of sparse responses to different odors (e.g claws that respond to different odors will appear negatively correlated).

D) Somatic responses as a function of responding claws. The height of each bar indicates the number of instances where *n* claws of a KC responded to an odor. The black fill denotes instances where there was also a somatic response in at least 2 of the 3 odor presentations. Blue curve shows the probability of somatic response as a function of number of responding claws.

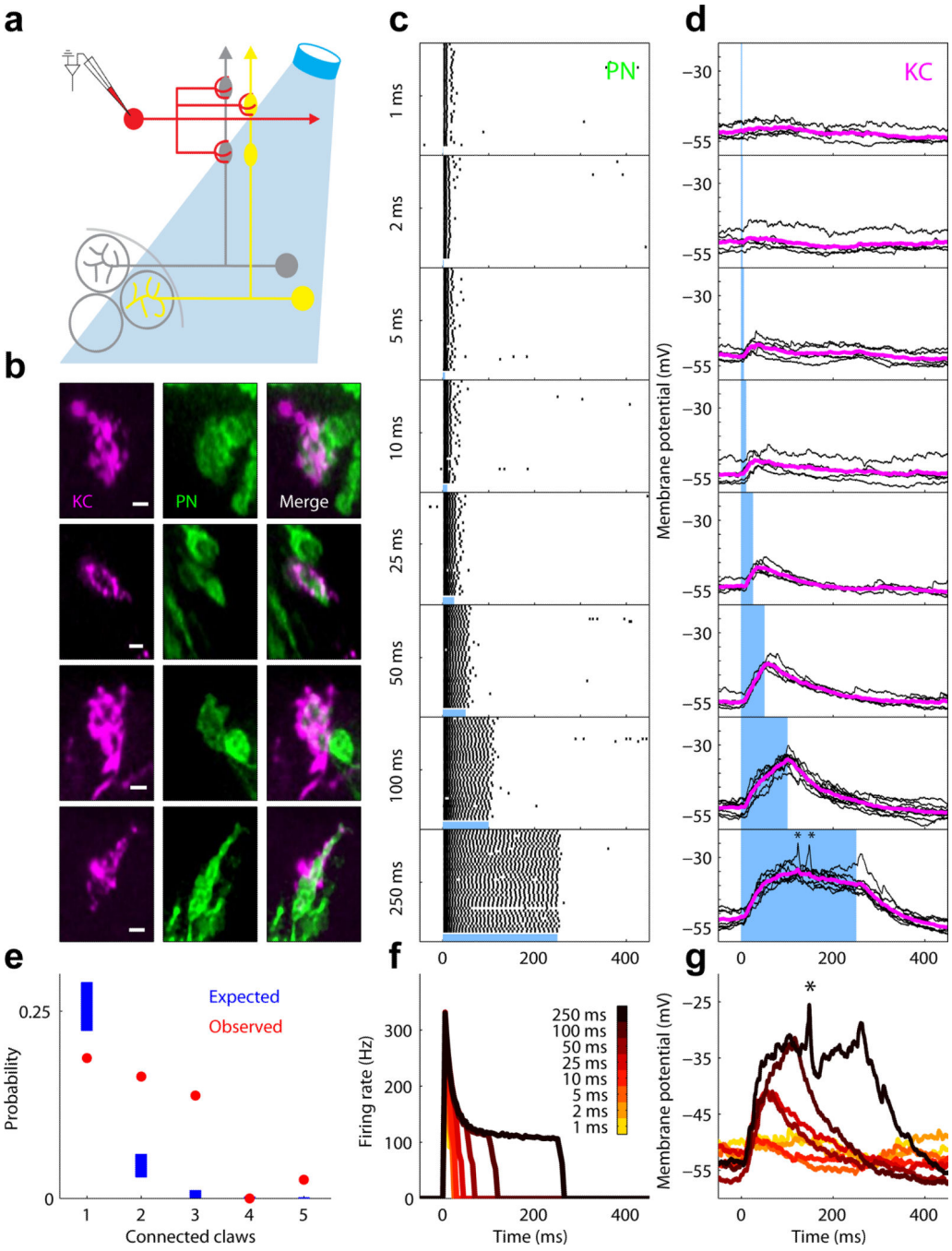

Figure 3. Detecting functional and anatomical connectivity between PNs and KCs using ChR2-based stimulation

a) Experimental schematic. ChR2-YFP was expressed in PNs innervating 3 of the 54 total glomeruli. Whole-cell KC recordings enabled detection of functional connectivity while intracellular dye-filling enabled characterization of anatomical connectivity

b) PN spiking responses to photostimulation.

c) Mean PN spiking rates (n=8) obtained with different photostimulation durations.

d) Postsynaptic responses of an example KC. Black traces indicate membrane potential recorded on a sample of individual trials, and magenta traces the mean (n=50 trials). Blue

shading indicates timing of photostimulation. Note that for this KC, the strongest stimulation evoked a response containing several spikes (denoted by an asterisk).

e) Overlay of single trial responses of a KC to increasing PN photostimulation, showing the increase in the evoked response, which culminates with a single spike (denoted by an asterisk). Same KC as in **d**.

f) Examples of PN to KC connections. Magenta: individual dye-filled KC claws. Green: YFP expressing PN boutons. Right: merge showing contact. Scale bar, 2 μM.

g) Comparison of the number of connected claws expected from random connectivity (blue bars) with the number observed experimentally (red dots). Blue bars denote the 99% confidence interval of the expected probability of each connection level, calculated using a binomial distribution with probability of connection p=0.05 (see Methods). Note that we observed 2 KCs connected via five claws in our sample of 39 connected cells, while the expected probability of observing 5 connected claws if connectivity were random is $p < 0.00001$.

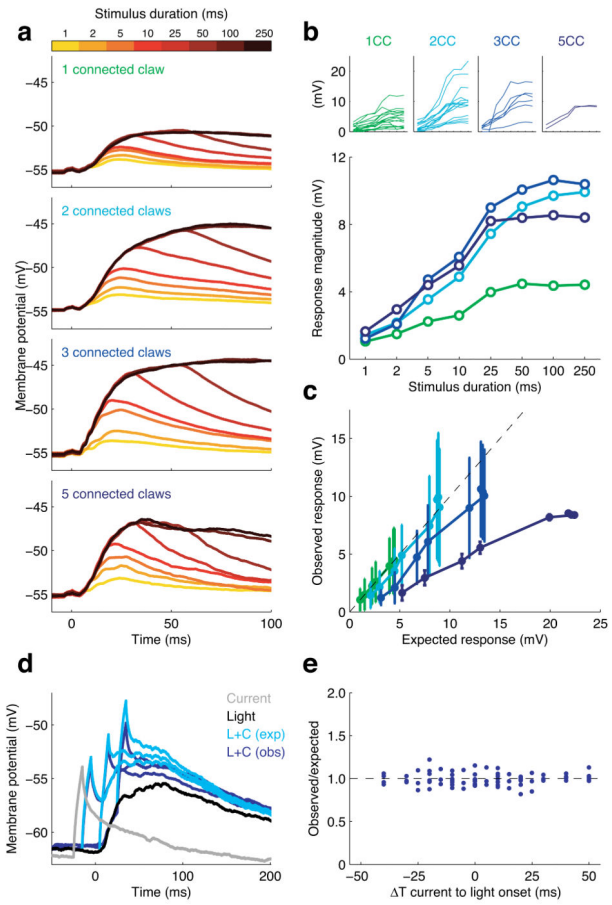

Figure 4. Additivity of synaptic input in KCs

a) Average timecourses of KC membrane potential in response to different durations of photostimulation (colorbar). KC responses are grouped according to the number of claws receiving direct PN input (connected claws, CC).

b) Response magnitudes increase with number of connected claws. Each line in the large panel depicts the mean peak responses of KCs with *n* connected claws. Insets above show the mean peak responses for each individual KC grouped by the number of connected claws.

c) Multiple synaptic inputs interact sublinearly in KCs. Expected response amplitudes were calculated for each duration of photostimulation (see panel **b**), assuming linear additivity of inputs across multiple claws. Experimentally observed responses for cells with 3 and 5 active claws fell below this linear prediction, indicating that multiple inputs interact sublinearly. Bars indicate ± SEM.

d) Overlay of KC membrane potential responses to combined photostimulation and somatic current injection, with current delivered at three different times relative to photostimulation. Observed responses (dark blue) closely matched those expected from linear summation (light blue) of isolated light and current responses.

e) Observed/Expected ratio for current and light stimulations across a range of different relative timings (n=7 KCs).

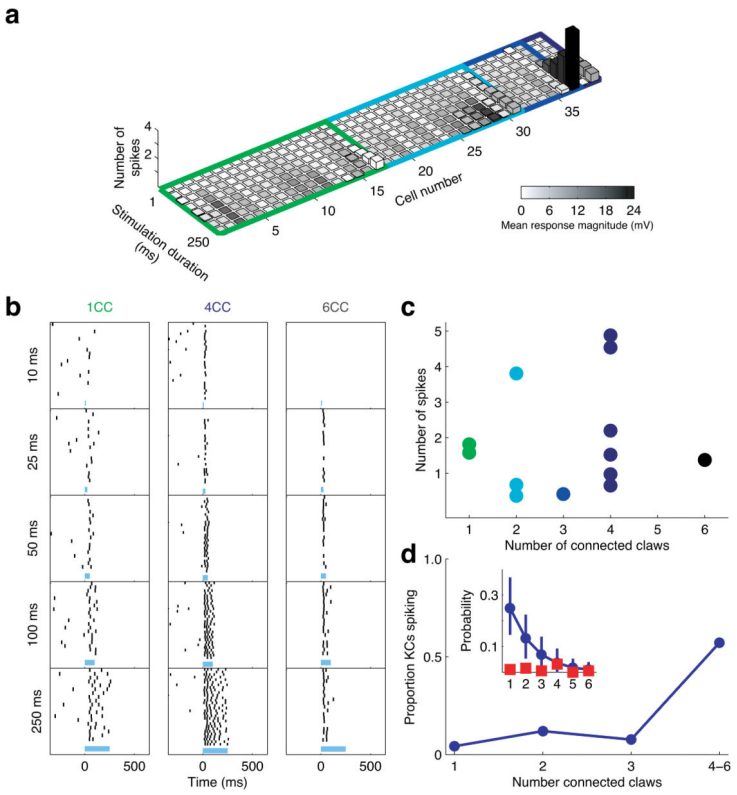

Figure 5. Kenyon cells require activation of multiple dendritic claws to spike

a) Histogram depicting both subthreshold (grayscale heatmap) and suprathreshold (z-axis) responses to PN photostimulation in synaptically connected KCs (n=39 KCs). Colored frames demarcate cells according to the number of connected claws; colors as in Fig. 4*b*. Bar height indicates number of spikes above spontaneous firing. Note the sparsity of spiking responses in this dataset, selected solely for synaptic connectivity to ChR2-expressing PNs, where only two cells showed reliable spiking responses (>0.5 sp/trial), one connected via 3 claws and another via 5.

b) Example KC spiking responses to photostimulation. In this dataset (distinct from **a**), n=191 KCs were recorded, and those exhibiting a reliable spiking response were selected for anatomical analysis to determine the number of connected claws for each cell. Each column of rasters shows an example of spiking activity observed for a particular level of connectivity. Duration of photostimulation shown at left and timing indicated by blue bar

c) Number of spikes evoked by photostimulation in KCs with different numbers of claws connected to ChR2-expressing PNs (n=13 spiking KCs).

d) Proportion of KCs exhibiting a spiking response across different levels of connectivity. KCs with 4 to 6 connected claws combined for analysis. Inset: Blue points indicate expected distribution of connectivity levels (99th percentile confidence interval), red points indicate observed frequency of spiking cells with different numbers of connected claws (see Methods).